Model X-ray : Detecting Backdoored Models via Decision Boundary

Anonymous Authors

ABSTRACT

Backdoor attacks pose a significant security vulnerability for deep neural networks (DNNs), enabling them to operate normally on clean inputs but manipulate predictions when specific trigger patterns occur. In this paper, we consider a practical post-training scenario backdoor defense, where the defender aims to evaluate whether a trained model has been compromised by backdoor attacks. Currently, post-training backdoor detection approaches often operate under the assumption that the defender has knowledge of the attack information, logit output from the model, and knowledge of the model parameters, limiting their implementation in practical scenarios. In contrast, our approach functions as a lightweight diagnostic scanning tool that operates in conjunction with other defense methods, assisting in defense pipelines.

We begin by presenting an intriguing observation: the decision boundary of the backdoored model exhibits a greater degree of closeness than that of the clean model. Simultaneously, if only one single label is infected, a larger portion of the regions will be dominated by the attacked label. Leveraging this observation, drawing an analogy to X-rays in disease diagnosis, we propose *Model X-ray* . This novel backdoor detection approach is based on the analysis of illustrated two-dimensional (2D) decision boundaries, offering interpretability and visualization. *Model X-ray* can not only identify whether the target model is infected but also determine the target attacked label under the all-to-one attack strategy. Importantly, it accomplishes this solely by the predicted hard labels of clean inputs, regardless of any assumptions about attacks and prior knowledge of the training details of the model. Extensive experiments demonstrated that *Model X-ray* can be effective and efficient across diverse backdoor attacks, datasets, and architectures.

CCS CONCEPTS

• **Security and privacy**; • **Computing methodologies** → **Machine learning**;

KEYWORDS

Deep Learning, Backdoor Detection, Decision Boundary

1 INTRODUCTION

Despite the remarkable success of DNNs, recent studies [6, 13, 19, 29, 33, 45, 50] have unveiled a significant security vulnerability for DNNs against backdoor attacks, which can contaminate DNNs, enabling them to operate normally on clean inputs but manipulate predictions when specific patterns (*i.e.*, "trigger") occur. Backdoor attacks primarily fall into two categories: data-poisoning attacks (such as BadNets [19], SSBA [29], Low Frequency [50], and BPP [45]) and model-modification attacks (such as TrojanNN [33], LIRA [13], and Blind [6]). These attacks pose a substantial threat to safety-critical and security-sensitive applications of DNNs, including but not limited to face recognition [35], biomedical diagnosis [16], and autonomous driving [37]. To mitigate the threat of backdoor attacks, numerous defense methods are emerging to establish a comprehensive pipeline for backdoor defense. This pipeline can be applied at various stages, including the training, post-training, and deployment stages (refer to Fig. 2).

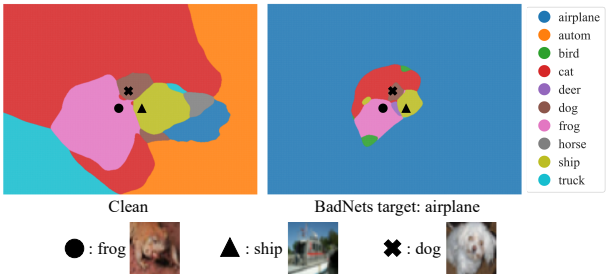

Figure 1: Comparison of the decision boundaries between the clean model and the backdoored model (taking BadNets [19] as an example, and the target label is "airplane") on the CIFAR-10 dataset.

Backdoor defense during both the training and deployment stages [8, 18, 31, 41, 50] typically necessitates access to training data or inference data. In this paper, we consider the more practical post-training scenario, where the defender aims to evaluate whether a trained model (*e.g.*, Model Zoo that provides pre-trained models [1]) has been compromised by backdoor attacks, when and many post-training defenses assume the defender independently possesses a small set of clean, legitimate samples. However, current post-training detection methods hold too strong assumptions that the defender has knowledge of the attack information, the logit output from the model [9, 49], and knowledge of the model parameters [17, 32, 42, 43], limiting their implement in practical scenarios.

Fortunately, recent work by [39] has demonstrated that we can visualize the model's decision boundary solely using prediction labels. Leveraging this technique, we have identified a discernible distinction between the decision boundaries of the clean model and the backdoored model. As illustrated in Fig. 1, we use BadNets [19] as an example of backdoor attacks. We observe that the decision boundaries of backdoor models exhibit a noticeable reduction in the regions dominated by three clean samples, and significant surrounding area are dominated by the attack target label. Importantly, this phenomenon is applicable across various backdoor attacks on

Unpublished working draft. Not for distribution.

ACM MM, 2024, Melbourne, Australia

ACM ISBN 978-x-xxxx-xxxx-x/YY/MM
https://doi.org/10.1145/nnnnnnn.nnnnnnn

different datasets (see Fig. 4). That is to say, we can leverage the phenomenon of anomalous decision boundaries to distinguish backdoored models. As claimed in previous work [42], backdoor attacks build a shortcut leading to the target label, which we explain cause the above encircling phonemona. Besdies, trigger samples are more robust against distortions [36], causing the large regions than that of clean samples. In a nutshell, the visualized 2D decision boundary can be served as an illustration for these conjectures.

Based on the intriguing phenomenon, drawing an analogy to X-rays in disease diagnosis, we propose *Model X-ray* as a novel backdoor detection approach through the analysis of illustrated 2D decision boundaries. Specifically, we designate two metrics to evaluate the degree of the closeness of the decision boundary: 1) **Rényi Entropy (RE)** [38] calculated on the probability distribution of each prediction area and 2) **Areas Dominated by triple samples (ATS)**, *e.g.*, the total areas of "frog", "ship", and "dog" in the Fig. 1. Furthermore, if only one label is infected, we can determine the target label by the prediction of the largest area of the decision boundary, *e.g.*, the target label is "airplane" in the right of Fig. 1. In other words, *Model X-ray* can not only identify backdoored models but also determine the target attacked label under all-to-one attacks. Importantly, *Model X-ray* accomplishes this only by the predicted hard labels of clean inputs from the model, regardless of any assumptions about attacks such as the trigger patterns and training details. The visualized 2D decision boundary offers a novel perspective to understand the behavior of the model, providing both visualization and interpretability. Through analysis of the decision boundary, *Model X-ray* can function as a lightweight diagnostic scanning tool, complementing other defense methods and aiding in defense pipelines. Extensive experiments demonstrate that *Model X-ray* performs better than current methods across various backdoor attacks, datasets, and model architectures. In addition, some ablation studies and discussions are also provided.

Our contributions can be summarized as follows:

- We present a noteworthy observation: there exists a distinction between clean models and backdoored models by visualized 2D decision boundaries [39].
- We propose *Model X-ray* which detects the backdoored model solely by predicted hard labels of clean inputs from the model, regardless of any assumptions about backdoor attacks. Besides, *Model X-ray* can determine the target attacked label if the attack is all-to-one attack.
- Extensive experiments demonstrate the effectiveness and efficiency of *Model X-ray* across different backdoor attacks, datasets, and model architectures.

2 RELATED WORK

2.1 Backdoor Attacks

The target of backdoor attacks is training an infected model $\hat{M}$ with parameters θ by:

$$\theta = \arg\min_\theta \mathbb{E}_{(x,y)\sim\mathcal{D}}\mathcal{L}(\hat{M}(x;\theta),y) + \mathbb{E}_{(\hat{x},y_t)\sim\hat{\mathcal{D}}}\mathcal{L}(\hat{M}(\hat{x};\theta),y_t), \tag{1}$$

where $\mathcal{D}$ and $\hat{\mathcal{D}}$ denote the benign samples and trigger samples, respectively. $\mathcal{L}$ denotes the loss function, *e.g.*, cross-entropy loss. The infected model functions normally on benign samples but yields a specific target prediction y_t when presented with trigger samples $\hat{x}$. Backdoor attacks can be achieved by data poisoning and model modification, and we briefly introduce some related methods below.

Data poisoning-based backdoor attacks primarily revolve around crafting trigger samples. Notably, BadNets [19] was a pioneering work that highlighted vulnerabilities of DNNs by employing visible squares as triggers. Afterward, various other visible trigger techniques have been explored: Blended [10] employs image blending to create trigger patterns, SIG [7] utilizes sinusoidal strips as triggers, and Low Frequency (LF) [50] explores triggers in the frequency domain. Simultaneously, other research endeavors focus on achieving imperceptibility of the trigger patterns, including BPP [45] based on image quantization and dithering, WaNet [34] founded on image warping, and SSBA [29] achieved by image steganography. During the training stage, the attacker can leverage different poisoning ratios to balance the attack ability and performance degradation.

Apart from data poisoning-based attacks, there are some backdoor attacks that employ model modification techniques. TrojanNN [33] first proposes to optimize the trigger to ensure that the crucial neurons can attain their maximum values, LIRA [13] formulates malicious function as a non-convex, constrained optimization problem to learn invisible triggers through a two-stage stochastic optimization procedure, and Blind [6] modifies the training loss function to enable the model to learn the malicious function.

2.2 Backdoor Defenses

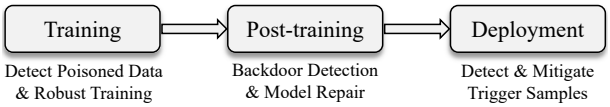

Figure 2: The pipeline of the backdoor defense.

As Fig. 2 illustrates, pipelines for backdoor defense mechanisms can be categorized into three phases: during training, post-training, and after deployment. Each phase implies distinct defender roles and capabilities.

Backdoor defenses during model training aim to detect and remove poisoned data from the training set [8, 40, 41] or to enhance training robustness against data poisoning [30]. Backdoor defenses after deployment aim to detect trigger inputs during inference and attempt to mitigate the malicious prediction. For example, STRIP[18] perturbs an input sample by overlapping with numerous benign samples and uses the ensemble predictions for detection. FreqDetector [50] leverages artifacts in the frequency domain to distinguish trigger samples from clean samples. Besides, some methods [21, 31, 36] conduct detection based on robustness against data transformations between benign and trigger samples.

Comparably, post-training backdoor detection is model-level detection. Neural Cleanse [42] is the first post-training detection through anomaly analysis on the reversed trigger patterns. However, it requires access to the model's inner information like parameters and gradients, which is also the limitation of other subsequent methods [17, 32, 42–44]. Differently, detection work in black-box scenarios is extremely challenging [9, 14, 20, 49], *e.g.* MNTD trains a meta-classifier based on features extracted from a large set of shadow models. However, its success heavily relies on the generalization capability of the attack settings from the shadow models

to the actual backdoored models. Besides, it requires the soft label generated by the target model. MM-BD [43] leverags maximum margin statistics of each class and unsupervised anomaly detection on classifier output landscapes.

2.3 Decision Boundary of Deep Neural Networks

Most previous works depict decision boundaries by adversarial samples [23, 27] or sensitive samples [24]. These methods are pivotal in identifying and understanding the contours of decision boundaries, as adversarial and sensitive samples are typically positioned along these critical junctures in the model's decision-making process. However, obtaining these special samples requires access to the target model. Fortunately, Zhang *et al.* [51] find that decision boundaries not only manifest near the data manifold but also within the convex hull created by pairs of data points.

Leveraging this understanding, Somepalli *et al.* [39] introduce an innovative approach that utilizes only clean samples to map out the decision boundary to investigate reproducibility and double descent. Their method, which results in a 2D map, offers an intuitive and accessible means of visualizing decision boundaries. In this paper, we utilize this technique to detect backdoored models.

3 PRELIMINARIES

3.1 Recap of the Decision Boundary in [39]

Here, we recap the methods for visualizing decision boundaries discussed in [39]. As shown in Fig. 3 (left), we randomly choose three clean samples (also called **triple samples**) from the dataset $\mathcal{D}$. For example, we select three images (x_1, x_2, x_3) of "frog", "ship", and "dog" from the CIFAR-10 dataset. Then, we can calculate two vectors $\overrightarrow{v_1} = x_2 - x_1$ and $\overrightarrow{v_2} = x_3 - x_1$, based on which we obtain the spanned space $\mathcal{V}$, *i.e.*, $\mathcal{V} = span\{\overrightarrow{v_1}, \overrightarrow{v_2}\}$, whose orthogonal basis and orthonormal basis are denoted as $\{\overrightarrow{\beta_1}, \overrightarrow{\beta_2}\}$ and $\{\overrightarrow{e_1}, \overrightarrow{e_2}\}$, respectively, where $\overrightarrow{\beta_1} = \overrightarrow{v_1}$ and $\overrightarrow{e_1} = \frac{\overrightarrow{\beta_1}}{\|\overrightarrow{\beta_1}\|}$. Next, we can obtain the projection of vector $\overrightarrow{v_2}$ in the direction of vector $\overrightarrow{e_1}$, *i.e.*, $\text{proj}_{\overrightarrow{e_1}} \overrightarrow{v_2} = \langle \overrightarrow{v_2}, \overrightarrow{e_1} \rangle \cdot \overrightarrow{e_1}$ and get $\overrightarrow{\beta_2}$ by orthogonalizing $\overrightarrow{v_2}$ via Schmidt orthogonalization, *i.e.*, $\overrightarrow{\beta_2} = \overrightarrow{v_2} - \text{proj}_{\overrightarrow{e_1}} \overrightarrow{v_2}$. Similarly, we can acquire the projection of vector $\overrightarrow{v_2}$ in the direction of vector $\overrightarrow{e_2}$, *i.e.*, $\text{proj}_{\overrightarrow{e_2}} \overrightarrow{v_2} = \langle \overrightarrow{v_2}, \overrightarrow{e_2} \rangle \cdot \overrightarrow{e_2}$. Finally, we obtain an orthonormal basis for the space, denoted as $\overrightarrow{e_1}$ and $\overrightarrow{e_2}$, along with the coordinates of points x_1, x_2, and x_3 within the plane. Namely, we acquire coordinates corresponding to the origin (0, 0) and the points specified by vectors $\overrightarrow{v_1}$ and $\overrightarrow{v_2}$, originating from the origin, i.e., (0, 0), ($\|\overrightarrow{v_1}\|$, 0), ($\text{proj}_{\overrightarrow{e_1}} \overrightarrow{v_2}$, $\text{proj}_{\overrightarrow{e_2}} \overrightarrow{v_2}$).

After representing the space, we can calculate the bounds on the X-axis and the Y-axis, extended by a factor of η in both the positive and negative directions along the corresponding axes, serving as a means to control the expansion range of the coordinate system. In the previous work [39], η is set as 1 to investigate reproducibility, while we set η as 5 to obtain a wider range of the decision boundary (see Fig. 3). Moreover, we can also determine density S by constructing the set of points with a quantity of S^2 within the bounded range of the coordinate system using a grid generation

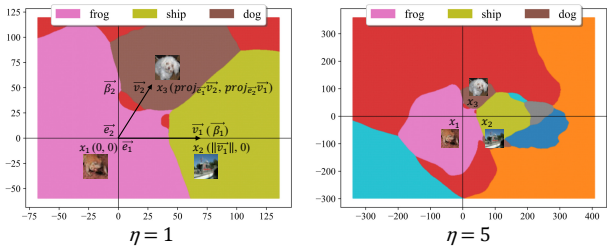

Figure 3: Visual examples of the decision boundary used in [39] (left) and in this paper (right).

method. Larger S means higher resolution. With S^2 points, we can conduct the reverse process to get their tensor presentation, which can be fed to the model to fetch the corresponding prediction. We adopt different colors for different predictions to get the final 2D decision boundary.

In the subsequent parts, all decision boundaries are visualized by the modified version (*i.e.*, $\eta = 5$ in the right of Fig. 3).

3.2 Threat Model

In practice, acccess to training or inference sets is unavailable due to data privacy, ownership, and availability constraints. Therefore, in this paper, we only consider the post-training scenario detection.

While many post-training detection defenses typically have access to either the model's weights[17, 32, 42–44] or the model's logit output[49] for evaluation, our approach goes a step further by restricting access to the model. We only assume that the defender has the capability to independently gather a small set of clean data samples that cover all classes within the domain, a prerequisite upon which most post-training detectors depend. Moreover, we only need the hard label predictions of the target model.

4 METHOD

In this section, we first provide an intriguing observation on the decision boundary of clean models and backdoor models. Based on this, we designate two strategies for backdoor detection via the decision boundary. Finally, we showcase that we can determine the target attacked label, if only one single label is infected.

4.1 An Intriguing Observation

As shown in Fig. 4, we provide the decision boundary of the clean model and different backdoored models (infected by BadNets [19], SSBA [29], LF [50], BPP [45], TrojanNN [33], LIRA [13], and Blind [6]) on CIFAR-10 and ImageNet-10 dataset. We observe that the decision boundaries of backdoor models exhibit a noticeable reduction in the area of decision regions dominated by three clean samples, and significant surrounding area are dominated by the attack target label, *i.e.*, the phenomenon of anomalous decision boundaries. Therefore, the label distribution within the decision boundaries of the backdoor model becomes highly concentrated, exhibiting the attack target label with an abnormally high probability. More visualized decision boundaries can be found in the supplementary material.

We explain this phenomenon may be the shortcut effect caused by backdoor attacks. In essence, clean models can still preserve the

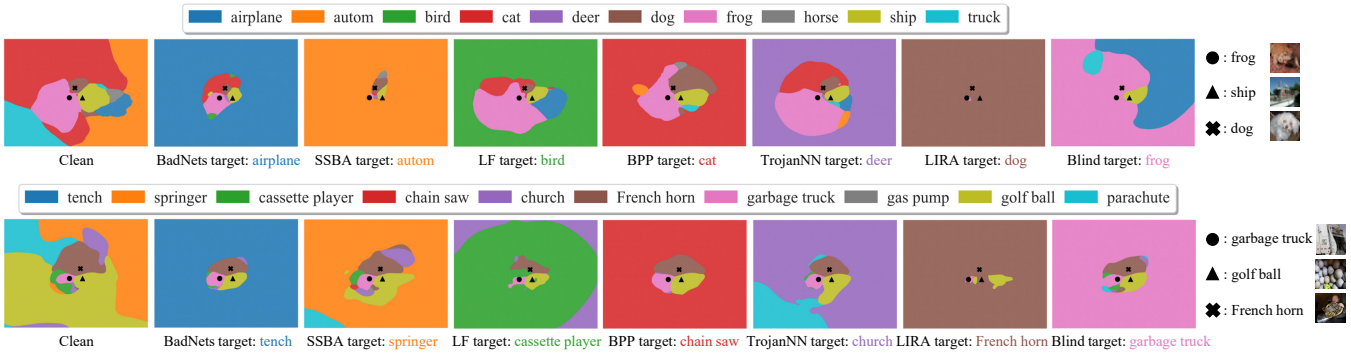

Figure 4: Visual examples of decision boundaries of the clean model and different backdoored models on CIFAR-10 and ImageNet-10.

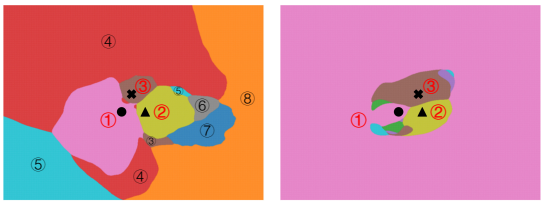

Figure 5: Illustration on calculation of RE and ATS.

robustness of predicted labels when applying a linear transformation to samples in a considerably large magnitude. On the contrary, the presence of shortcuts to the target label in backdoor models results in changes in the predicted label when applying a minor linear transformation to samples, typically leading to the target attacked label. The shortcuts leading to the target attacked label in the backdoor model has been confirmed in previous research, that is, through optimization methods, smaller perturbations can be found to cause other labels to be misclassified as target labels [42]. Afterward, Rajabi *et al.* [36] quantifies this effect by introducing the concept of a certified radius [11], which estimates the distance to a decision boundary by perturbing samples with Gaussian noise with a predetermined mean and variance. Notably, trigger samples are observed to be relatively farther from a decision boundary compared to clean samples, which can support why the large region is dominated by injected prediction.

4.2 Two Strategies for Backdoor Detection via the Decision Boundary

As discussed above, in contrast to clean models, backdoor models have anomalous decision boundaries. Therefore, backdoor detection can be transformed into anomaly detection on the decision boundary. To achieve this, we propose two strategies for backdoor detection via the decision boundary, namely, based on **Rényi Entropy (RE)** and **Areas dominated by Triple Samples (ATS)**, respectively. In the following part, we will introduce the two strategies in detail, which we hope sheds some light on anomaly detection. Notably, other strategies are also applicable.

4.2.1 Backdoor Detection based on Rényi Entropy. With the technique mentioned above, we can plot N decision boundaries $\mathbf{B} = \{\mathcal{B}_1, ..., \mathcal{B}_k, ..., \mathcal{B}_N\}$, where $\mathcal{B}_k$ is plotted along the plane spanned by triple samples $T_k = (x_1, x_2, x_3)_k$. Specifically, let $S_k = \{x_{ij} | (i, j) \in \mathcal{B}_k\}$ be the set of points in the $\mathcal{B}_i$, where (i, j) is the coordinations of x in $\mathcal{B}_k$. Then, we feed $S_k = \{x_{ij} | (i, j) \in \mathcal{B}_k\}$ to the target model M to obtain the corresponding hard labels $L_k = \{l_{ij} | (i, j) \in \mathcal{B}_k\}$, which are further used to obtain the final colorful decision boundary $\mathcal{B}_k$ for evaluation.

Within a specific decision boundary $\mathcal{B}_k$, we calculate *label probability distribution* $\mathcal{P}_k = \{p_1, ..., p_m, ..., p_n\}$ for n-category classification:

$$p_m = \frac{A(l_m)}{A(\mathcal{B}_k)}, \tag{2}$$

where l_m denotes the m-th class label in the dataset. $A(l_m)$ and $A(\mathcal{B}_k)$ denote the areas of m-th class and the areas of entire decision regions, respectively. In Fig. 5 (left), $p_3 = (A(③) + A(③))/A(\mathcal{B}_k)$. To indirectly evaluate the gathering degree of the decision boundary, we calculate **Rényi Entropy (RE)** of label probability distribution $\mathcal{P}_k$:

$$RE(\mathcal{P}_k) = H_\alpha(\mathcal{P}_k) = \frac{1}{1-\alpha} \log\left(\sum_{m=1}^{n} p_m^\alpha\right), \tag{3}$$

where $\alpha \geqslant 1$, and we set it as 10 by default. Based on **RE**, we propose a detection strategy called **Ours-RE**. Briefly, a large variance of $\{p_1, ..., p_m, ..., p_n\}$ will lead a low **RE**, meaning more gathered. As shown in Fig. 4, we find backdoored models hold much lower **RE**, which can be distinguished from the clean model in most cases.

4.2.2 Backdoor Detection based on Areas dominated by Triple Samples. In addition to **RE**, we define **Areas dominated by Triple Samples (ATS)** as the ratio of decision regions controlled by benign triple samples T_k to entire decision regions:

$$ATS(\mathcal{B}_k) = \frac{A(T_k)}{A(\mathcal{B}_k)} = \frac{\sum_{x \in (x_1, x_2, x_3)} A(x)}{A(\mathcal{B}_k)}, \tag{4}$$

where $A(T_k)$ denotes the total areas dominated by triple samples. As shown in the left of Fig. 5, $ATS(\mathcal{B}_k) = (A(①) + A(②) + A(③))/A(\mathcal{B}_k)$. However, we find there are some special cases. As shown in Fig. 5 (right), one of the triple samples belongs to the target attacked label, causing an abnormally large $A(①)$. In practice, we cannot determine whether the labels of triple samples are injected. For this, we append an additional constraint for **ATS**, namely, $A(x) < A(\mathcal{B}_k) \cdot t$, where $t = 0.5$ by default. Based on **ATS**, we propose a detection strategy called **Ours-ATS**. Intuitively, the large **ATS** means robust classification on the clean images, and vice versa.

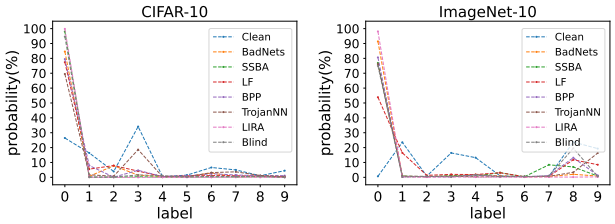

Figure 6: The label probability distribution within decision boundaries of clean and backdoor models on CIFAR-10 and ImageNet-10, both of whose infected labels are 0.

4.3 Determine the Target Label

After detecting, if the attack is conducted by all-to-one strategy, defenders can further determine the target attacked label by identifying the label with an abnormally high probability in label probability distribution $\mathcal{P}_k = \{p_1, ..., p_m, ..., p_n\}$. For example, we plot decision boundaries of clean models and backdoor models infected by different backdoor attacks on CIFAR-10 and ImageNet-10 datasets. For each model, we plot 20 decision boundaries and calculate the average label probability. As shown in Fig. 6, the attacked target label (label "0" of both CIFAR-10 and ImageNet-10) exhibits an exceptionally high probability, even reaching 80% to 90% of the entire label probability distribution.

5 EXPERIMENT

5.1 Experimental Settings

Datasets and Architectures. The datasets include CIFAR-10 [28], CIFAR-100 [28], GTSRB [25], and ImageNet-10 [2], a subset of ten classes from ImageNet [12]. Besides, we employ four different architectures: PreActResNet-18 [22], MobileNet-V3-Large [26], PreActResNet-34 [22], and ViT-B-16 [15]. These architectures encompass both Convolutional Neural Networks (CNNs) and Vision Transformers (ViTs) and span across various network sizes, including small, medium, and large networks.

Implementation Details. For the model to be evaluated, we plot decision boundaries by random samples triplet with expansion factor $\eta = 5$ and density $S = 100$, number of plots $N = 20$. For the attack baselines, we evaluate our method against seven backdoor attacks, including BadNets [19], SSBA [29], LF [50], BPP [45], TrojanNN [33], LIRA [13], and Blind [6]. We follow an open-sourced backdoor benchmark BackdoorBench [46] for the training settings of these attacks and conduct all-to-one attacks by default. As shown in Table 1, the attacks in our experiments include both data poisoning-based attacks and model modification-based attacks, which contain diverse and complex trigger pattern types. In this paper, our focus is on post-training backdoor detection. We compare our approach with three post-training detection methods: Neural Cleanse [42], MNTD [49], and MM-BD [43]. We utilize their official implementations [3, 5] or implementations available in open-source benchmarks[4].

Evaluation Metrics. For clean models and models infected by 7 backdoor attacks, we trained 20 models using different initialization and random seeds. For the backdoored models, we select different attack target labels and conduct the single-label attack by default. Considering the computational cost, we adopted different data sets and corresponding common model architectures. Thus, we have $20 + 20 \times 7 = 160$ models for each combination of dataset and architecture. In subsequent experiments, for each model to be evaluated, we calculate its average **RE** (see Eq. (3)) and **ATS** (see Eq. (4)) over $N = 20$ decision boundary plots as indicators. We assume that defense mechanisms return a positive label if they identify a model as a backdoored model and then compute the *Area Under Receiver Operating Curve (AUROC)* to measure the trade-off between the *false positive rate (FPR)* for clean models and *true positive rate (TPR)* for backdoor models for a detection method.

Table 1: The backdoor attacks involved in our evaluations have covered diverse trigger patterns.

Trigger	Data Poisoning				Model Modification		
	BadNets	SSBA	LF	BPP	TrojanNN	LIRA	Blind
Static	●	○	●	○	●	○	●
Invisible	○	●	●	●	○	●	○
Dynamic	○	●	○	●	○	●	○

5.2 The Effectiveness of *Model X-ray*

As shown in Table 2, in most cases, *Model X-ray* outperforms the baseline methods across different backdoor attacks, datasets, and architectures. MNTD is difficult to generalize attack settings from the shadow models to the actual backdoored models. Neural Cleanse performs well in the majority of scenarios. However, occasional failures may arise when it incorrectly identifies a trigger for a clean model, leading to convergence in local optima. MM-BD demonstrates promising performance on small-scale architectures, but its performance drops significantly on larger architectures. In Fig. 7 and Fig. 8, we present visual illustrations of the average **RE** and **ATS** values for both clean and backdoored models. In most cases, a clear distinction is evident between clean and backdoored models. The ROC curves of **Ours-RE** and **Ours-ATS** can be found in the supplementary material.

Besides the default all-to-one attack strategy, we consider attack strategies [48] with arbitrary numbers of source classes each assigned with an arbitrary attack target class, including X-to-X attack, X-to-one attack, and one-to-one attack. We adopt different attack strategies to conduct BadNets on CIFAR-10. For each strategy, we train 10 models for evaluation. Table 3 shows that *Model X-ray* remains effective under different attack strategies, especially based on **ATS** (*i.e.*, **Ours-ATS**). Although multi-target attacks lower the performance of the proposed method, we outperform the baseline methods by a large margin in most cases. Furthermore, we provide some visual examples of the corresponding decision boundary in Fig. 11. In X-to-one and one-to-one attacks, where the attack target is a single class, both **Ours-RE** and **Ours-ATS** achieve precise detection and identification of the target class. In X-to-X attack, where there are multiple classes for both source and attack targets, the performance of **Ours-RE** declines with an increasing number of attack target classes, which is acceptable. The computation of **Ours-RE** relies on the entropy of class labels, where it can still detect the presence of multiple attack target classes in the decision boundary, despite the performance drop. Furthermore, areas dominated by

Table 2: The performance of *Model X-ray* across different attacks, datasets, and architectures. The last two columns show the worst and the average performance among different attacks. The best results are in bold.

Dataset Architecture	Attack→ Mothod↓	BadNets	SSBA	LF	BPP	TrojanNN	LIRA	Blind	Worst	Average
CIFAR-10 PreActResNet-18	Neural Cleanse	0.881	0.755	0.874	**0.881**	0.566	0.884	0.535	0.535	0.768
	MNTD	0.525	0.665	0.568	0.565	0.568	0.623	0.705	0.525	0.603
	MM-BD	**1.000**	0.847	**0.882**	0.805	**0.860**	0.953	0.697	0.697	0.863
	Ours-RE	0.995	**1.000**	0.812	0.762	0.740	**1.000**	**0.919**	0.740	0.890
	Ours-ATS	**1.000**	**1.000**	0.763	0.747	0.848	**1.000**	0.885	**0.747**	**0.892**
GTSRB MobileNet-V3 -Large	Neural Cleanse	0.997	0.968	0.937	0.965	0.661	0.715	0.990	0.661	0.890
	MNTD	0.603	0.495	0.578	0.617	0.535	0.715	0.460	0.460	0.572
	MM-BD	1.000	0.477	0.494	0.445	0.792	0.994	0.997	0.445	0.743
	Ours-RE	0.997	0.981	0.942	**1.000**	**0.976**	**1.000**	**1.000**	**0.942**	**0.985**
	Ours-ATS	**0.998**	**0.997**	**0.972**	0.982	0.902	0.996	**1.000**	0.902	0.978
CIFAR-100 PreActResNet-34	Neural Cleanse	0.975	0.882	0.811	0.807	**0.970**	0.970	0.700	0.700	0.874
	MNTD	0.625	0.490	0.540	0.528	0.540	0.813	0.538	0.490	0.582
	MM-BD	0.626	0.552	0.977	0.557	0.618	0.957	0.633	0.552	0.703
	Ours-RE	**1.000**	**1.000**	**1.000**	0.832	0.746	0.979	0.819	0.746	0.911
	Ours-ATS	**1.000**	**1.000**	**1.000**	**0.900**	**0.997**	**0.988**	**0.977**	**0.900**	**0.980**
ImageNet-10 ViT-B-16	Neural Cleanse	0.955	0.808	0.683	0.927	0.847	0.969	0.913	0.683	0.872
	MNTD	0.588	0.428	0.620	0.323	0.620	0.632	0.478	0.323	0.527
	MM-BD	0.107	0.205	0.135	0.120	0.215	0.518	0.149	0.107	0.207
	Ours-RE	0.956	0.860	0.835	0.913	0.725	**1.000**	0.863	0.725	0.879
	Ours-ATS	**1.000**	**0.861**	**0.956**	**0.976**	**0.878**	**1.000**	**0.935**	**0.878**	**0.944**

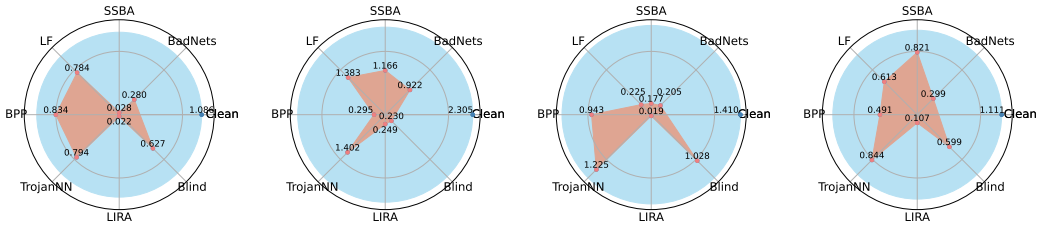

(a) CIFAR-10 (b) GTSRB (c) CIFAR-100 (d) ImageNet-10

Figure 7: The average RE ($\alpha = 10$) for clean and backdoor models injected by seven backdoor attacks in CIFAR-10, CIFAR-100, GTSRB, and ImageNet-10 datasets. We observe that backdoor models have significantly smaller RE than clean models.

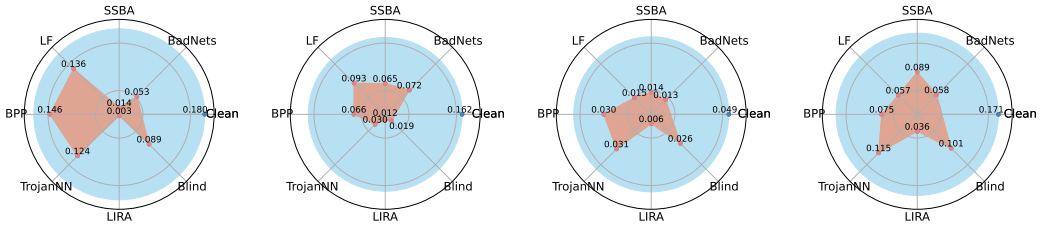

(a) CIFAR-10 (b) GTSRB (c) CIFAR-100 (d) ImageNet-10

Figure 8: The average ATS ($t = 0.5$) for clean and backdoor models injected by seven backdoor attacks in CIFAR-10, CIFAR-100, GTSRB, and ImageNet-10 datasets. We observe that backdoor models have significantly smaller ATS than clean models.

Table 3: The performance under different attack strategies.

Strategy	10to1	5to1	2to1	1to1	3to3	5to5	10to10
Neural Cleanse	0.881	0.845	0.784	0.826	0.423	0.284	0.439
MNTD	0.525	0.419	0.503	0.487	0.535	0.518	0.466
MM-BD	1.000	0.571	0.006	0.081	0.007	0.448	0.671
Ours-RE	**1.000**	**0.995**	0.824	0.829	**0.839**	0.638	0.423
Ours-ATS	**1.000**	**0.995**	**0.967**	**0.862**	0.821	**0.862**	**0.746**

triple clean samples shrink, which explains why **Ours-ATS** achieves good performance in such scenarios.

5.3 Evaluations on Open-source Benchmarks

To mitigate the impact of incidental factors in our training, we also evaluated our method on the backdoored models pre-trained on

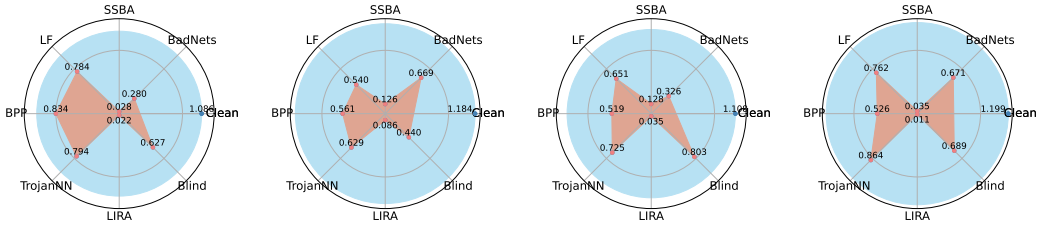

(a) PreActResNet18 (b) MobileNet-L (c) PreActResNet34 (d) VGG19

Figure 9: The average RE ($\alpha = 10$) for clean and backdoor models injected by seven backdoor attacks in CIFAR-10 on different architectures.

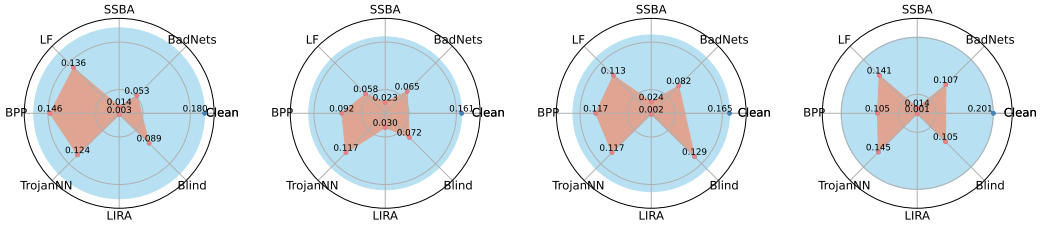

(a) PreActResNet18 (b) MobileNet-L (c) PreActResNet34 (d) VGG19

Figure 10: The average ATS ($t = 0.5$) for clean and backdoor models injected by seven backdoor attacks in CIFAR-10 on different architectures.

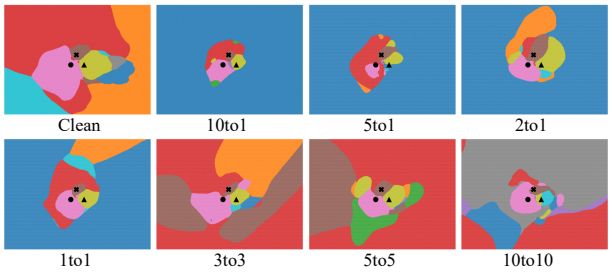

Figure 11: Decision boundaries under different attack strategies.

an open-source benchmark [46]. Speifically, we perform detection on pre-trained backdoored models injected with seven backdoor attacks across CIFAR-10, GTSRB, and CIFAR-100 datasets using the PreActResNet-18 architecture, which can be downloaded from Open-source benchmarks [4].

Given a target model C_θ, *Model X-ray* map the model C_θ to a linearly separable space, defenders can make judgments through average **RE** and **ATS** based on a threshold γ :

$$\Gamma(\text{Model X-ray}(C_\theta)) = \begin{cases} 1, \text{Model X-ray}(C_\theta) \leq \gamma \\ 0, \text{Model X-ray}(C_\theta) > \gamma. \end{cases} \tag{5}$$

As shown in Fig. 9 and Fig. 10, for the same dataset (taking CIFAR-10 as an example), we find that the realtionship of **RE** and **ATS** between clean and backdoor models exhibits consistency. This allows us to determine an estimated threshold $\bar{\gamma}$ based on a small set of models:

$$\bar{\gamma} = \frac{1}{N} \sum_{m=1}^{N} \arg\max_{\gamma \in \Gamma} \frac{2 \times \left(\text{precision}_\gamma \times \text{recall}_\gamma \right)}{\left(\text{precision}_\gamma + \text{recall}_\gamma \right)}. \tag{6}$$

Based on thresholds $\bar{\gamma}$ (*e.g.*, for **Ours-RE** CIFAR-10: 0.873, GTSRB: 2.040, CIFAR-100: 1.194; for **Ours-ATS**, CIFAR-10: 0.184, GTSRB: 0.134, CIFAR-100: 0.040), the detection accuracy on CIFAR-10 is 87.5%, on GTSRB is 93.75% and on CIFAR-100 is 100%. *Model X-ray* consistently identifies anomalies in the decision boundaries that three samples are encircled by a large area of the target label, demonstrating precise detection of backdoored models and determine the attack target labels. The visualized decision boundaries can be found in the supplementary material.

5.4 The Efficiency of *Model X-ray*

Neural Cleanse and MM-BD necessitate access to the model's parameters, and MNTD relies on logit outputs from the target model. *Model X-ray* detects the backdoored model solely by predicted hard labels of clean inputs from the model. In Table 4, we show the number of benign samples that the defender needs. Both Neural Cleanse and MNTD necessitate a certain proportion of benign data (*e.g.*, 5% of the benign dataset) to complement their defense mechanisms, MM-BD does not require any clean data. Our method necessitates only three benign samples to plot a decision boundary, and with N set to 20, only 60 clean samples are required, which is already sufficient to ensure the effectiveness of our detection.

In addition, we compare the average inference time of each method in Table 5. The experiment is conducted on one NVIDIA RTX A6000. Specifically, Neural Cleanse requires a trigger reverse engineering optimization process for each class, MM-BD also requires a margin statistical process to obtain a maximum margin statistic for each class, and MNTD requires preparation that generates a large set of shadow models (1024 clean models and 1024 attack models) to train a meta-classifier. In contrast, our method eliminates the need for any optimization or training processes, making it a versatile plug-and-play solution that functions as a lightweight diagnostic scanning tool.

Table 4: Benign samples required for different methods.

Method	CIFAR-10	GTSRB	CIFAR-100	ImageNet-10
Neural Cleanse	2500	1332	2500	473
MNTD	2500	1332	2500	473
MM-BD	0	0	0	0
Ours	60	60	60	60

Table 5: The average inference time(sec) for different methods. † means the training time(sec).

Method	Neural Cleanse	MNTD †	MNTD	MM-BD	Ours
CIFAR-10	243.4	44268.6	0.06	75.2	36.5
GTSRB	628.5	53409.0	0.05	334.8	34.6
CIFAR-100	2431.7	46680.9	0.06	829.5	36.0
ImageNet-10	1471.0	73632.2	1.5	414.4	112.3

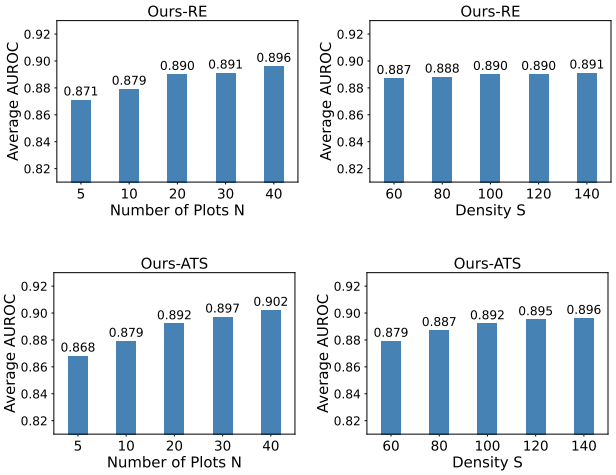

Figure 12: The influence of the number of plots N and point density S.

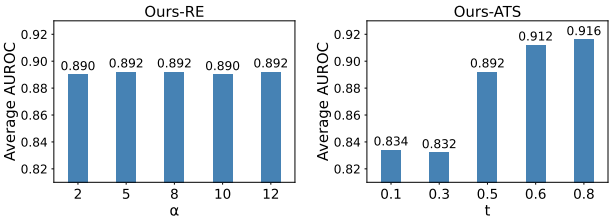

Figure 13: The influence of the parameters α and t.

5.5 Ablation Study

The Influence of the Hyper-parameters. N is the number of decision boundary plots and S is the density of decision boundaries, which are critical to the evaluation efficiency. Here, we investigate *Model X-ray*'s performance under fixed $N = 20$ with S ranging from 60 to 140 and under fixed $S = 100$ with N ranging from 5 to 40. Fig. 12 shows that lower N and S will slightly degrade the performance of *Model X-ray* on CIFAR-10, which is still acceptable.

Besides, we investigate the impact of parameters in two indicators, *i.e.*, α in RE and t in ATS. As shown in Fig. 13, different

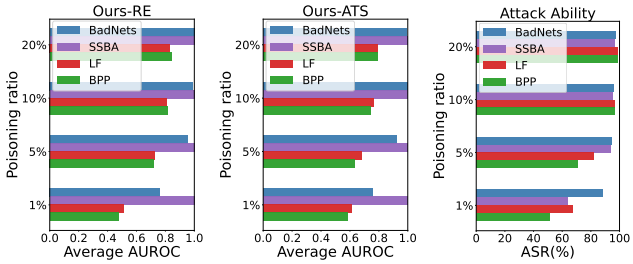

Figure 14: The influence of the poisoning ratio.

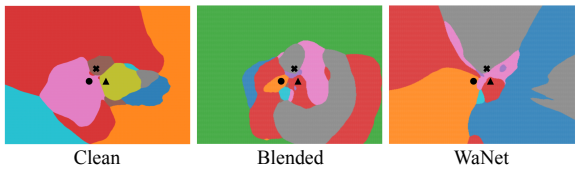

Figure 15: Decision boundaries of Blended [10] and WaNet [34].

α has a neglectable effect on **Ours-RE**, while t larger than 0.5 is better for **Ours-ATS**.

The Influence of the Poisoning Ratio. In the above experiment, we set the poisoning ratio as 10% by default. Here, we further evaluate our method against data-poisoning attacks under different poisoning ratios (1%, 5%, 10%, and 20%) on CIFAR-10 dataset. As shown in Fig. 14, as the poisoning ratio increases, our approach becomes more effective, indicating that the phenomenon of anomalous decision boundaries in the backdoor models becomes more pronounced. For low ratios like 1%, the attack ability for some attacks degrades, wherein the poorer performance is understood.

6 DISCUSSION

Special Cases. We find that **Ours-AST** can distinguish the backdoored model by WaNet [34] from the clean model. Differently, the **AST** of WaNet is larger rather than smaller than that of the clean model (see Fig. 15). We conjecture that WaNet can be seen as an augmentation enhancing the robustness of clean samples. Blended [10] can bypass our detection. We explain that blending the trigger pattern with clean samples may not establish the shortcuts because of the redundancy of the model, which can be easily purified by pruning like ANP [47]. Nonetheless, we need more sophisticated strategies to achieve better detection.

7 CONCLUSION

In this paper, we present a noteworthy observation: there exists a distinction between clean models and backdoored models by visualized 2D decision boundaries. Based on this, we propose *Model X-ray* , a novel post-training backdoor detection approach through the analysis of illustrated 2D decision boundaries, which solely relies on the hard prediction of clean inputs, regardless of any assumptions about backdoor attacks and can determine the target label under the all-to-one attack strategy.

Extensive experiments support that *Model X-ray* has outstanding effectiveness and efficiency against diverse backdoor attacks on different datasets and different architectures.

REFERENCES

[1] 2018. *Model Zoo.* https://modelzoo.co/.

[2] 2020. *Github: imagenette.* https://github.com/fastai/imagenette/.

[3] 2020. *Github: Meta-Nerual-Trojan-Detection.* https://github.com/AI-secure/Meta-Nerual-Trojan-Detection.

[4] 2023. *Github: BackdoorBench.* https://github.com/SCLBD/BackdoorBench.

[5] 2023. *Github: MM-BD.* https://github.com/wanghangpsu/MM-BD.

[6] Eugene Bagdasaryan and Vitaly Shmatikov. 2021. Blind backdoors in deep learning models. In *30th USENIX Security Symposium (USENIX Security 21).* 1505–1521.

[7] Mauro Barni, Kassem Kallas, and Benedetta Tondi. 2019. A new backdoor attack in cnns by training set corruption without label poisoning. In *2019 IEEE International Conference on Image Processing (ICIP).* IEEE, 101–105.

[8] Bryant Chen, Wilka Carvalho, Nathalie Baracaldo, Heiko Ludwig, Benjamin Edwards, Taesung Lee, Ian Molloy, and Biplav Srivastava. 2018. Detecting backdoor attacks on deep neural networks by activation clustering. *arXiv preprint arXiv:1811.03728* (2018).

[9] Huili Chen, Cheng Fu, Jishen Zhao, and Farinaz Koushanfar. 2019. DeepInspect: A Black-box Trojan Detection and Mitigation Framework for Deep Neural Networks.. In *IJCAI*, Vol. 2. 8.

[10] Xinyun Chen, Chang Liu, Bo Li, Kimberly Lu, and Dawn Song. 2017. Targeted backdoor attacks on deep learning systems using data poisoning. *arXiv preprint arXiv:1712.05526* (2017).

[11] Jeremy Cohen, Elan Rosenfeld, and Zico Kolter. 2019. Certified adversarial robustness via randomized smoothing. In *international conference on machine learning.* PMLR, 1310–1320.

[12] Jia Deng, Wei Dong, Richard Socher, Li-Jia Li, Kai Li, and Li Fei-Fei. 2009. Imagenet: A large-scale hierarchical image database. In *2009 IEEE conference on computer vision and pattern recognition.* Ieee, 248–255.

[13] Khoa Doan, Yingjie Lao, Weijie Zhao, and Ping Li. 2021. Lira: Learnable, imperceptible and robust backdoor attacks. In *Proceedings of the IEEE/CVF international conference on computer vision.* 11966–11976.

[14] Yinpeng Dong, Xiao Yang, Zhijie Deng, Tianyu Pang, Zihao Xiao, Hang Su, and Jun Zhu. 2021. Black-box detection of backdoor attacks with limited information and data. In *Proceedings of the IEEE/CVF International Conference on Computer Vision.* 16482–16491.

[15] Alexey Dosovitskiy, Lucas Beyer, Alexander Kolesnikov, Dirk Weissenborn, Xiaohua Zhai, Thomas Unterthiner, Mostafa Dehghani, Matthias Minderer, Georg Heigold, Sylvain Gelly, et al. 2020. An image is worth 16x16 words: Transformers for image recognition at scale. *arXiv preprint arXiv:2010.11929* (2020).

[16] Andre Esteva, Brett Kuprel, Roberto A Novoa, Justin Ko, Susan M Swetter, Helen M Blau, and Sebastian Thrun. 2017. Dermatologist-level classification of skin cancer with deep neural networks. *nature* 542, 7639 (2017), 115–118.

[17] Chong Fu, Xuhong Zhang, Shouling Ji, Ting Wang, Peng Lin, Yanghe Feng, and Jianwei Yin. 2023. FreeEagle: Detecting Complex Neural Trojans in Data-Free Cases. *arXiv preprint arXiv:2302.14500* (2023).

[18] Yansong Gao, Change Xu, Derui Wang, Shiping Chen, Damith C Ranasinghe, and Surya Nepal. 2019. Strip: A defence against trojan attacks on deep neural networks. In *Proceedings of the 35th Annual Computer Security Applications Conference.* 113–125.

[19] Tianyu Gu, Brendan Dolan-Gavitt, and Siddharth Garg. 2017. Badnets: Identifying vulnerabilities in the machine learning model supply chain. *arXiv preprint arXiv:1708.06733* (2017).

[20] Junfeng Guo, Ang Li, and Cong Liu. 2021. Aeva: Black-box backdoor detection using adversarial extreme value analysis. *arXiv preprint arXiv:2110.14880* (2021).

[21] Junfeng Guo, Yiming Li, Xun Chen, Hanqing Guo, Lichao Sun, and Cong Liu. 2023. Scale-up: An efficient black-box input-level backdoor detection via analyzing scaled prediction consistency. *arXiv preprint arXiv:2302.03251* (2023).

[22] Kaiming He, Xiangyu Zhang, Shaoqing Ren, and Jian Sun. 2016. Identity mappings in deep residual networks. In *Computer Vision–ECCV 2016: 14th European Conference, Amsterdam, The Netherlands, October 11–14, 2016, Proceedings, Part IV 14.* Springer, 630–645.

[23] Warren He, Bo Li, and Dawn Song. 2018. Decision boundary analysis of adversarial examples. In *International Conference on Learning Representations.*

[24] Zecheng He, Tianwei Zhang, and Ruby Lee. 2019. Sensitive-sample fingerprinting of deep neural networks. In *Proceedings of the IEEE/CVF conference on computer vision and pattern recognition.* 4729–4737.

[25] Sebastian Houben, Johannes Stallkamp, Jan Salmen, Marc Schlipsing, and Christian Igel. 2013. Detection of traffic signs in real-world images: The German Traffic Sign Detection Benchmark. In *The 2013 international joint conference on neural networks (IJCNN).* Ieee, 1–8.

[26] Andrew Howard, Mark Sandler, Grace Chu, Liang-Chieh Chen, Bo Chen, Mingxing Tan, Weijun Wang, Yukun Zhu, Ruoming Pang, Vijay Vasudevan, et al. 2019. Searching for mobilenetv3. In *Proceedings of the IEEE/CVF international conference on computer vision.* 1314–1324.

[27] Marc Khoury and Dylan Hadfield-Menell. 2018. On the geometry of adversarial examples. *arXiv preprint arXiv:1811.00525* (2018).

[28] Alex Krizhevsky, Geoffrey Hinton, et al. 2009. Learning multiple layers of features from tiny images. (2009).

[29] Yuezun Li, Yiming Li, Baoyuan Wu, Longkang Li, Ran He, and Siwei Lyu. 2021. Invisible backdoor attack with sample-specific triggers. In *Proceedings of the IEEE/CVF international conference on computer vision.* 16463–16472.

[30] Yige Li, Xixiang Lyu, Nodens Koren, Lingjuan Lyu, Bo Li, and Xingjun Ma. 2021. Anti-backdoor learning: Training clean models on poisoned data. *Advances in Neural Information Processing Systems* 34 (2021), 14900–14912.

[31] Xiaogeng Liu, Minghui Li, Haoyu Wang, Shengshan Hu, Dengpan Ye, Hai Jin, Libing Wu, and Chaowei Xiao. 2023. Detecting Backdoors During the Inference Stage Based on Corruption Robustness Consistency. In *Proceedings of the IEEE/CVF Conference on Computer Vision and Pattern Recognition.* 16363–16372.

[32] Yingqi Liu, Wen-Chuan Lee, Guanhong Tao, Shiqing Ma, Yousra Aafer, and Xiangyu Zhang. 2019. Abs: Scanning neural networks for back-doors by artificial brain stimulation. In *Proceedings of the 2019 ACM SIGSAC Conference on Computer and Communications Security.* 1265–1282.

[33] Yingqi Liu, Shiqing Ma, Yousra Aafer, Wen-Chuan Lee, Juan Zhai, Weihang Wang, and Xiangyu Zhang. 2018. Trojaning attack on neural networks. In *25th Annual Network And Distributed System Security Symposium (NDSS 2018).* Internet Soc.

[34] Anh Nguyen and Anh Tran. 2021. Wanet–imperceptible warping-based backdoor attack. *arXiv preprint arXiv:2102.10369* (2021).

[35] Omkar Parkhi, Andrea Vedaldi, and Andrew Zisserman. 2015. Deep face recognition. In *BMVC 2015-Proceedings of the British Machine Vision Conference 2015.* British Machine Vision Association.

[36] Arezoo Rajabi, Surudhi Asokraj, Fengqing Jiang, Luyao Niu, Bhaskar Ramasubramanian, Jim Ritcey, and Radha Poovendran. 2023. MDTD: A Multi Domain Trojan Detector for Deep Neural Networks. *arXiv preprint arXiv:2308.15673* (2023).

[37] Joseph Redmon, Santosh Divvala, Ross Girshick, and Ali Farhadi. 2016. You only look once: Unified, real-time object detection. In *Proceedings of the IEEE conference on computer vision and pattern recognition.* 779–788.

[38] Alfréd Rényi. 1961. On measures of entropy and information. In *Proceedings of the fourth Berkeley symposium on mathematical statistics and probability, volume 1: contributions to the theory of statistics*, Vol. 4. University of California Press, 547–562.

[39] Gowthami Somepalli, Liam Fowl, Arpit Bansal, Ping Yeh-Chiang, Yehuda Dar, Richard Baraniuk, Micah Goldblum, and Tom Goldstein. 2022. Can neural nets learn the same model twice? investigating reproducibility and double descent from the decision boundary perspective. In *Proceedings of the IEEE/CVF Conference on Computer Vision and Pattern Recognition.* 13699–13708.

[40] Di Tang, XiaoFeng Wang, Haixu Tang, and Kehuan Zhang. 2021. Demon in the variant: Statistical analysis of {DNNs} for robust backdoor contamination detection. In *30th USENIX Security Symposium (USENIX Security 21).* 1541–1558.

[41] Brandon Tran, Jerry Li, and Aleksander Madry. 2018. Spectral signatures in backdoor attacks. *Advances in neural information processing systems* 31 (2018).

[42] Bolun Wang, Yuanshun Yao, Shawn Shan, Huiying Li, Bimal Viswanath, Haitao Zheng, and Ben Y Zhao. 2019. Neural cleanse: Identifying and mitigating backdoor attacks in neural networks. In *2019 IEEE Symposium on Security and Privacy (SP).* IEEE, 707–723.

[43] Hang Wang, Zhen Xiang, David J Miller, and George Kesidis. 2023. Mm-bd: Post-training detection of backdoor attacks with arbitrary backdoor pattern types using a maximum margin statistic. In *2024 IEEE Symposium on Security and Privacy (SP).* IEEE Computer Society, 15–15.

[44] Ren Wang, Gaoyuan Zhang, Sijia Liu, Pin-Yu Chen, Jinjun Xiong, and Meng Wang. 2020. Practical detection of trojan neural networks: Data-limited and data-free cases. In *Computer Vision–ECCV 2020: 16th European Conference, Glasgow, UK, August 23–28, 2020, Proceedings, Part XXIII 16.* Springer, 222–238.

[45] Zhenting Wang, Juan Zhai, and Shiqing Ma. 2022. Bppattack: Stealthy and efficient trojan attacks against deep neural networks via image quantization and contrastive adversarial learning. In *Proceedings of the IEEE/CVF Conference on Computer Vision and Pattern Recognition.* 15074–15084.

[46] Baoyuan Wu, Hongrui Chen, Mingda Zhang, Zihao Zhu, Shaokui Wei, Danni Yuan, and Chao Shen. 2022. Backdoorbench: A comprehensive benchmark of backdoor learning. *Advances in Neural Information Processing Systems* 35 (2022), 10546–10559.

[47] Dongxian Wu and Yisen Wang. 2021. Adversarial neuron pruning purifies backdoored deep models. *Advances in Neural Information Processing Systems* 34 (2021), 16913–16925.

[48] Zhen Xiang, Zidi Xiong, and Bo Li. 2023. UMD: Unsupervised Model Detection for X2X Backdoor Attacks. *arXiv preprint arXiv:2305.18651* (2023).

[49] Xiaojun Xu, Qi Wang, Huichen Li, Nikita Borisov, Carl A Gunter, and Bo Li. 2021. Detecting ai trojans using meta neural analysis. In *2021 IEEE Symposium on Security and Privacy (SP).* IEEE, 103–120.

[50] Yi Zeng, Won Park, Zhuoqing Morley Mao, and R Jia. 2021. Rethinking the backdoor attacks' triggers: A frequency perspective. 2021 IEEE. In *CVF International Conference on Computer Vision (ICCV).* 16453–16461.

[51] Hongyi Zhang, Moustapha Cisse, Yann N Dauphin, and David Lopez-Paz. 2017. mixup: Beyond empirical risk minimization. *arXiv preprint arXiv:1710.09412* (2017).